

This discussion paper is/has been under review for the journal The Cryosphere (TC).
Please refer to the corresponding final paper in TC if available.

Combining damage and fracture mechanics to model calving

J. Krug^{1,2}, J. Weiss^{1,2}, O. Gagliardini^{1,2,3}, and G. Durand^{1,2}

¹CNRS, LGGE, 38041 Grenoble, France

²Univ. Grenoble Alpes, LGGE, 38041 Grenoble, France

³Institut Universitaire de France, Paris, France

Received: 4 March 2014 – Accepted: 13 March 2014 – Published: 24 March 2014

Correspondence to: J. Krug (jean.krug@ujf-grenoble.fr)

Published by Copernicus Publications on behalf of the European Geosciences Union.

1631

Abstract

Calving of icebergs is a major negative component of polar ice-sheet mass balance. We present a new calving modeling framework relying on both continuum damage mechanics and linear elastic fracture mechanics. This combination accounts for both the slow sub-critical surface crevassing and fast propagation of crevasses when calving occurs. First, damage of the ice occurs over long timescales and enhances the viscous flow of ice. Then brittle fracture propagation happens downward, over very short timescales, in ice considered as an elastic medium. The model is validated on Helheim Glacier, South-West Greenland, one of the most monitored fast-flowing outlet glacier. This allows to identify sets of model parameters giving a consistent response of the model and producing a dynamic equilibrium in agreement with observed stable position of the Helheim ice front between 1930 and today.

1 Introduction

Over the last decades, discharge of ice from Greenland and Antarctic ice sheets strongly increased (Shepherd et al., 2012), due to either a larger submarine melting, or an increasing rate of calving. Recent observations have shown that the ice loss is, in average, equally distributed between these two sink terms despite some regional differences (Rignot et al., 2010; Depoorter et al., 2013). Ice loss by iceberg calving has been evaluated to 1321 ± 144 gigatonnes per year for Antarctica in 2013 (Depoorter et al., 2013) and 357 gigatonnes per year for Greenland between 2000 and 2005 (Rignot and Kanagaratnam, 2006). These figures could become more important, as the front destabilization can exert a strong positive feedback on glacier dynamics. Indeed, the abrupt collapse of the front can destabilize the whole glacier, leading to both the thinning and so the acceleration of upstream ice through the loss of buttressing, and thus increasing again the discharge (Gagliardini et al., 2010). The collapse of Larsen B ice shelf in 2002 (Scambos et al., 2004) or the disintegration of the floating tongue of

1632

Jakobshavn Isbrae, on the West coast of Greenland ice sheet the same year (Joughin et al., 2008a) are two examples of the impact of such perturbations on the behaviour of a glacier. In the sake of projecting ice sheet evolution, a deep understanding and representation of the processes occurring at the front are necessary, especially those

5 concerning iceberg calving.
 Among the several studies undertaken to model calving, the most used criterion is the one proposed by Nye (1957), according to whom the ability for a glacier to calve depends on the equilibrium between longitudinal stretching (opening term) and cryostatic pressure (closing term). This criterion has been used by several authors (e.g. Mottram and Benn, 2009; Nick et al., 2010; Otero et al., 2010; Nick et al., 2013) with successful results in representing the front variations of some major greenlandic and antarctic outlet glaciers. However, this model is based on a simple stress balance combined to an empirical criterion for calving. Consequently, it does not account for some physical aspects, such as the stress concentration at the tip of crevasses, or the crevasse depth, and so it may assess inaccurately the ice discharge in case of prognostic simulations.

15 Another approach to model calving has been done using particles models (Bassis and Jacobs, 2013; Åström et al., 2013). These models show interesting behaviours on describing the calving processes and the iceberg distribution, but are today inappropriate to describe large-scale ice-sheet flow due to their non-continuous approach.

20 For a few years, some authors have focused on continuum damage mechanics in order to represent both the development of micro-defects in the ice to the apparition of macro-scale crevasses, and their effects on the viscous behaviour of the ice while keeping a continuum approach. Initially applied to the deformation of metals (Kachanov, 1958), damage mechanics has been recently applied to ice dynamics to study the apparition of a single crevasse (Pralong et al., 2003; Pralong and Funk, 2005; Duddu and Waisman, 2013) or to average crevasse fields (Borstad et al., 2012). On the other hand, the elastic representation of fracturing processes using linear elastic fracture mechanics (van der Veen, 1998a, b) has been employed to described the calving event itself, characterized by a rapid propagation of surface and bottom crevasses through the ice.

1633

This approach has been rarely used in ice-sheet numerical modeling, however, as the representation of crevasses requires a high mesh refinement usually difficult to reach when modeling large glaciological bodies.

5 Here we consider a combined approach between damage mechanics and fracture mechanics. The proposed physically-based calving model can cover both the accumulation of damage as the ice is transported through the glacier, and the critical fracture propagation in the vicinity of the calving front. The slow development of damage represents the long timescales evolution of purely viscous ice, while the use of fracture mechanics allows to consider calving events occurring at short timescales, for which the ice can be considered as a purely elastic medium. The description of the physics implemented is presented in Sect. 2, covering the damage initiation and its development, the fracture propagation and its arrest criterion. In Sect. 3, sensitivity tests are carried on Helheim Glacier, and results are discussed.

2 Physics of the model

15 2.1 Governing equations for ice flow

2.1.1 Ice flow and rheology

We consider an incompressible, isothermal and gravity-driven ice-flow in which the ice exhibits a non-linear viscosity. The ice flow is ruled by the Stokes equations (i.e. Navier–Stokes equations without any inertial term), meaning the momentum and the mass balance:

$$\text{div}(\boldsymbol{\sigma}) + \rho_i \mathbf{g} = 0 \quad (1)$$

$$\text{div}(\mathbf{u}) = 0 \quad (2)$$

25 where $\boldsymbol{\sigma}$ represents the Cauchy stress tensor, \mathbf{g} the gravity force vector, ρ_i the density of ice and \mathbf{u} the velocity vector. The Cauchy stress tensor can be expressed as a func-

1634

point loads along the crack length. In our case, instead of considering the value of the along-flow component of the deviatoric stress tensor at the tip of the crack, we multiplied it by the weight function $\beta(z, d, H)$ at each vertical coordinate and integrated it over the initial crevasse depth (Labbens et al., 1974). This way, the effect of a stress profile of arbitrary shape on the stress intensity factor can be taken into account.

In LEFM theory, a fracture is able to propagate downward in the ice if the stress intensity factor is higher than the fracture toughness K_{Ic} . The toughness is a property of the material and strongly depends on the porosity in the ice. Several experiments have been carried out to relate the value of K_{Ic} to this porosity (Fischer et al., 1995; Rist et al., 1996; Schulson and Duval, 2009). Among the range of values between $0.1 \text{ MPa m}^{1/2}$ and $0.4 \text{ MPa m}^{1/2}$, we choose a constant value of $0.2 \text{ MPa m}^{1/2}$. Sensitivity to this value will be discussed in Sect. 3.3.4.

The weight function $\beta(z, d, H)$ depends on the geometry of the crevasse, and so it depends on the considered problem. Among the weight functions for various crack and notch geometries, that has been proposed, we use the one corresponding to an edge crack in an infinite width plate (Glinka, 1996), in two dimensions. A complete description of the weight function and an illustration of the geometry is given in Fig. 2 and Appendix A.

2.3.2 Critical damage contour and fracture initiation

From Eq. (16), it is easily understandable that an initiation of crevasse propagation requires a combination of both sufficient tensile stress and large enough initial crevasse depth to exceed fracture toughness. In our model, the size of pre-existing flaws is dictated by a contour of critical damage on the near-surface of the glacier, where damage reaches a critical value D_c . For application to the LEFM theory, we consider that the depth of this damaged layer corresponds to the initial crevasse depth d (see Fig. 3). One must keep in mind that this value of D_c is another threshold which needs to be set. The sensitivity of the model to this parameter will be tested in Sect. 3.

1643

Compared to the work of van der Veen (1998a, b), we do not consider the presence of water-filled crevasses for the initiation of crack propagation, nor the formation of basal crevasses. It has been shown that water-filled crevasses are able to propagate the full thickness of the glacier as soon as the level of water in the crevasse exceeds several meters. Without this feature, our model is sufficient to provide a lower bound for crevasse propagation. It is worth noting, however, that the introduction of such a mechanism in our framework would be straightforward, once the water level within crevasses can be defined independently.

2.3.3 Fracture arrest

Once the conditions for fracture initiation are fulfilled, we consider that the crevasse propagates vertically. In van der Veen (1998b), crevasses propagate downward as long as the inequation $K_I \geq K_{Ic}$ is satisfied, thus assuming that $K_I = K_{Ic}$ represents both a crack propagation and a crack arrest criterion. Such arrest criterion is probably misleading, as the stress intensity factor at arrest, though non-zero, is always lower than the stress intensity factor at propagation (Ravi-Chandar and Knauss, 1984), mostly as dynamical effects have to be taken into account for the arrest condition. Therefore, following Ravi-Chandar, we use a crevasse arrest criterion: $K_I < K_{Ia}$, with $K_{Ia} = \alpha K_{Ic}$ and $0 < \alpha < 1$. The value of α for ice is unknown. In the following, we arbitrarily set α to 0.5. Sensitivity to this value will be discussed in Sect. 3.3.4.

In this simplified LEFM framework, calving would theoretically occur only if K_I remains larger than K_{Ia} down to the bottom of the glacier. However, as the result of cryostatic pressure and/or boundary conditions (hydrostatic pressure), K_I becomes negative before reaching $d = H$. To overcome this inconsistency, authors have proposed alternative criteria. Benn et al. (2007a) proposed a first-order approach considering that calving of the aerial part of the glacier occurs when a surface crevasse reaches the sea-level. This criterion is supported by two observations. Firstly, Motyka (1997) showed that calving of the aerial part occurs when the crevasse reaches the sea level, usually followed by the calving of the subaqueous part. Secondly, a surface crevasse

1644

old, and damaging never happens. The Damage enhancement factor B is related to the rate at which the damage increases, once the damage criterion χ is positive. This value is particularly difficult to evaluate, especially because it does not lay on laboratory experiments or observations. Thus, we choose a large range [0.5, 3]. However, one must note that this parameter should have a value which keeps the stress field in the vicinity of the damage envelope, once the stress has been released by damaging. The critical damage value D_c has already been documented (Pralong and Funk, 2005; Borstad et al., 2012; Duddu and Waisman, 2013). According to their values, we set our range within [0.4, 0.6]. The number of computed simulations was 250.

3.3.2 Calibration of the model: spin-up

Damage can be produced anywhere in the glacier. As we need to obtain a steady state for the damage field, it is necessary to let the damage created upstream be advected to the front. This spin-up lasts 8 years. During this period, the front is maintained at its initial position, without submarine frontal melting, and the procedure of calving is not activated. Once the steady state is obtained, the front is released, the frontal melting is prescribed and the calving procedure is activated.

3.3.3 Model response

As mentioned in Andresen et al. (2011), over the last century, Helheim Glacier has probably undergone several advance and retreat cycles, and observations of sand deposits imply a variation of the terminus around less than 10 km. The knowledge about the potential triggering mechanisms for retreat cycles is still poor: according to Joughin et al. (2008b) and Andresen et al. (2011), this retreat may have been forced by an enhanced summer temperature, and higher ocean water temperature, although sensitivity of calving to temperature remains unclear.

For these reasons, we did not try to reproduce the precise chronology of the Helheim's recent retreat in this paper. Instead, we study the dynamical behaviour of the

1649

model with respect to the different sets of parameters, and try to distinguish between unrealistic and realistic behaviours. The simulations presented in the previous sections were run during 4 years after the spin-up. Among the 250 sets of parameters, the model response can be split in 3 classes, illustrated in Fig. 6. The blue curve on this figure represents a case where the calving almost never happened, and where the glacier advances too much, creating a floating tongue of several kilometers. The yellow curve illustrates a case where the calving occurs too quickly, leading to a front retreat far upstream. The red curve represents a case consistent against observations, where the front of the glacier is punctuated by irregular calving events, forcing the glacier to keep its extent in an acceptable range of values.

This classification in three classes of behaviour can be generalized to the 250 simulations. In order to eliminate aberrant behaviour, we prescribe a sanity-check, by considering plausible sets of parameters as the ones which lead to a simulated front position within the range [340 km, 350 km]. The results are represented in Fig. 7, in the space of parameter $(B, \overline{\sigma_{th}})$. On this figure, we distinguished once again the same three classes, blue plus signs, yellow crosses and red diamonds, representing respectively the case where the front exceeds 350 km, the case where the front retreats more inland than 340 km, and the case where the front remains within this range. The curves illustrated in Fig. 6 are represented here by closed circles using the same colorscale.

The steadily advance of the front without or with few calving events can be explained considering the couple $(B, \overline{\sigma_{th}})$. These simulations are characterized by a low value of B and/or a high value of $\overline{\sigma_{th}}$. This means that either the incrementation of damage is too low, or the stress threshold is too high to allow damage initiation. In these cases, damage production is not sufficient to reach the calving criterion $D = D_c$, whatever its chosen value. In addition, when $\overline{\sigma_{th}}$ is too high, the damage may only increases in the area where the traction is very high, meaning at the top of bumps, in the immediate vicinity of the surface. As a consequence, the damage does never reach a sufficient depth to trigger calving.

1650

- Åström, J. A., Riikilä, T. I., Tallinen, T., Zwinger, T., Benn, D., Moore, J. C., and Timonen, J.: A particle based simulation model for glacier dynamics, *The Cryosphere*, 7, 1591–1602, doi:10.5194/tc-7-1591-2013, 2013. 1633
- Bassis, J. and Jacobs, S.: Diverse calving patterns linked to glacier geometry, *Nat. Geosci.*, 6, 833–836, 2013. 1633, 1646
- 5 Benn, D. I., Hulton, N. R., and Mottram, R. H.: “Calving laws”, “sliding laws” and the stability of tidewater glaciers, *Ann. Glaciol.*, 46, 123–130, 2007a. 1644
- Benn, D. I., Warren, C. R., and Mottram, R. H.: Calving processes and the dynamics of calving glaciers, *Earth-Sci. Rev.*, 82, 143–179, 2007b. 1640, 1645, 1655
- 10 Bevan, S. L., Luckman, A. J., and Murray, T.: Glacier dynamics over the last quarter of a century at Helheim, Kangerdlugssuaq and 14 other major Greenland outlet glaciers, *The Cryosphere*, 6, 923–937, doi:10.5194/tc-6-923-2012, 2012. 1646
- Borstad, C. P., Khazendar, A., Larour, E., Morlighem, M., Rignot, E., Schodlok, M. P., and Seroussi, H.: A damage mechanics assessment of the Larsen B ice shelf prior to collapse: Toward a physically-based calving law, *Geophys. Res. Lett.*, 39, L18502, doi:10.1029/2012GL053317, 2012. 1633, 1637, 1641, 1649
- 15 Cook, S. J.: Environmental Controls on Calving in Grounded Tidewater Glaciers, Ph.D. thesis, Swansea University, Swansea, UK, 2012. 1646
- Depoorter, M., Bamber, J., Griggs, J., Lenaerts, J., Ligtenberg, S., van den Broeke, M., and Moholdt, G.: Calving fluxes and basal melt rates of Antarctic ice shelves, *Nature*, 502, 82–92, 2013. 1632
- Duddu, R. and Waisman, H.: A temperature dependent creep damage model for polycrystalline ice, *Mech. Mater.*, 46, 23–41, 2012. 1639
- Duddu, R. and Waisman, H.: A nonlocal continuum damage mechanics approach to simulation of creep fracture in ice sheets, *Comput. Mech.*, 51, 1–14, 2013. 1633, 1639, 1649
- 25 Durand, G., Gagliardini, O., De Fleurian, B., Zwinger, T., and Le Meur, E.: Marine ice sheet dynamics: hysteresis and neutral equilibrium, *J. Geophys. Res.-Earth*, 114, F03009, doi:10.1029/2008JF001170, 2009. 1636
- Favier, L., Gagliardini, O., Durand, G., and Zwinger, T.: A three-dimensional full Stokes model of the grounding line dynamics: effect of a pinning point beneath the ice shelf, *The Cryosphere*, 6, 101–112, doi:10.5194/tc-6-101-2012, 2012. 1636
- 30 Fischer, M., Alley, R., and Engelder, T.: Fracture toughness of ice and firn determined from the modified ring test, *J. Glaciol.*, 41, 383–394, 1995. 1643

1657

- Gagliardini, O., Durand, G., Zwinger, T., Hindmarsh, R., and Le Meur, E.: Coupling of ice-shelf melting and buttressing is a key process in ice-sheets dynamics, *Geophys. Res. Lett.*, 37, L14501, doi:10.1029/2010GL043334, 2010. 1632, 1648
- Gagliardini, O., Weiss, J., Duval, P., and Montagnat, M.: On Duddu and Waisman (2012a, b) concerning continuum damage mechanics applied to crevassing and icebergs calving, *J. Glaciol.*, 59, 797–798, 2013a. 1639
- 5 Heinke, J., Ostberg, S., Schaphoff, S., Frieler, K., Müller, C., Gerten, D., Meinshausen, M., and Lucht, W.: A new climate dataset for systematic assessments of climate change impacts as a function of global warming, *Geosci. Model Dev.*, 6, 1689–1703, doi:10.5194/gmd-6-1689-2013, 2013b. 1645
- 10 Gillet-Chaulet, F., Gagliardini, O., Seddik, H., Nodet, M., Durand, G., Ritz, C., Zwinger, T., Greve, R., and Vaughan, D. G.: Greenland ice sheet contribution to sea-level rise from a new-generation ice-sheet model, *The Cryosphere*, 6, 1561–1576, doi:10.5194/tc-6-1561-2012, 2012. 1648
- 15 Glinka, G.: Development of weight functions and computer integration procedures for calculating stress intensity factors around cracks subjected to complex stress fields, *Stress and Fatigue-Fracture Design*, Petersburg Ontario, Canada, Progress Report, 1, 1, 1996. 1643, 1655
- Hayhurst, D.: Creep rupture under multi-axial states of stress, *J. Mech. Phys. Solids*, 20, 381–382, 1972. 1639
- 20 Howat, I. M., Joughin, I., and Scambos, T. A.: Rapid changes in ice discharge from Greenland outlet glaciers, *Science*, 315, 1559–1561, 2007. 1646, 1647, 1648
- Jay-Allemand, M., Gillet-Chaulet, F., Gagliardini, O., and Nodet, M.: Investigating changes in basal conditions of Variegated Glacier prior to and during its 1982–1983 surge, *The Cryosphere*, 5, 659–672, doi:10.5194/tc-5-659-2011, 2011. 1636
- 25 Joughin, I., Das, S. B., King, M. A., Smith, B. E., Howat, I. M., and Moon, T.: Seasonal speedup along the western flank of the Greenland Ice Sheet, *Science*, 320, 781–783, 2008a. 1633
- Joughin, I., Howat, I., Alley, R. B., Ekstrom, G., Fahnestock, M., Moon, T., Nettles, M., Truffer, M., and Tsai, V. C.: Ice-front variation and tidewater behavior on Helheim and Kangerdlugssuaq Glaciers, Greenland, *J. Geophys. Res.-Earth*, 113, F01004, doi:10.1029/2007JF000837, 2008b. 1646, 1649, 1653
- 30

1658

- Jouvet, G., Picasso, M., Rappaz, J., Huss, M., and Funk, M.: Modelling and Numerical Simulation of the Dynamics of Glaciers Including Local Damage Effects, *Mathematical Modelling of Natural Phenomena*, 6, 263–280, 2011. 1637
- Kachanov, L.: Time of the rupture process under creep conditions, *Isv. Akad. Nauk. SS R. Otd Tekh. Nauk*, 8, 26–31, 1958. 1633, 1637
- 5 Labbens, R., Pellissier-Tanon, A., and Heliot, J.: Application de la théorie linéaire de la mécanique de la rupture aux structures métalliques épaisses – Méthodes pratiques de calcul des facteurs d'intensité de contrainte, *Rev. Phys. Appl.*, 9, 587–598, 1974. 1642, 1643
- Lemaitre, J., Chaboche, J., and Germain, P.: *Mécanique des Matériaux Solides*, vol. 7, Dunod, Paris, 1988. 1637, 1638
- 10 Luckman, A., Murray, T., De Lange, R., and Hanna, E.: Rapid and synchronous ice-dynamic changes in East Greenland, *Geophys. Res. Lett.*, 33, L03503, doi:10.1029/2005GL025428, 2006. 1646
- Ma, Y., Gagliardini, O., Ritz, C., Gillet-Chaulet, F., Durand, G., and Montagnat, M.: Enhancement factors for grounded ice and ice shelves inferred from an anisotropic ice-flow model, *J. Glaciol.*, 56, 805–812, 2010. 1635
- 15 Mottram, R. H. and Benn, D. I.: Testing crevasse-depth models: a field study at Breioamerkurjokull, Iceland, *J. Glaciol.*, 55, 746–752, 2009. 1633, 1641, 1652
- Motyka, R.: Deep-water calving at Le Conte Glacier, southeast Alaska, *Byrd Polar Res. Cent. Rep.*, 15, 115–118, 1997. 1644
- 20 Murakami, S. and Ohno, N.: A continuum theory of creep and creep damage, in: *Creep in Structures*, Springer, Tempaku-cho, Toyohashi 440, Japan, 422–444, 1981. 1638
- Nath, P. and Vaughan, D.: Subsurface crevasse formation in glaciers and ice sheets, *J. Geophys. Res.-Sol. Ea.*, 108, 2020, 2003. 1641
- 25 Nick, F. M., Vieli, A., Howat, I. M., and Joughin, I.: Large-scale changes in Greenland outlet glacier dynamics triggered at the terminus, *Nat. Geosci.*, 2, 110–114, 2009. 1646, 1647, 1648
- Nick, F. M., van der Veen, C. J., Vieli, A., and Benn, D. I.: A physically based calving model applied to marine outlet glaciers and implications for the glacier dynamics, *J. Glaciol.*, 56, 781–794, 2010. 1633, 1645
- 30 Nick, F. M., Vieli, A., Andersen, M. L., Joughin, I., Payne, A., Edwards, T. L., Pattyn, F., and van de Wal, R. S.: Future sea-level rise from Greenland's main outlet glaciers in a warming climate, *Nature*, 497, 235–238, 2013. 1633

1659

- Nye, J.: The distribution of stress and velocity in glaciers and ice-sheets, *P. Roy. Soc. Lond A Mat.*, 239, 113–133, 1957. 1633
- Otero, J., Navarro, F. J., Martin, C., Cuadrado, M. L., and Corcuera, M. I.: A three-dimensional calving model: numerical experiments on Johnsons Glacier, Livingston Island, Antarctica, *J. Glaciol.*, 56, 200–214, 2010. 1633
- 5 Pralong, A. and Funk, M.: Dynamic damage model of crevasse opening and application to glacier calving, *J. Geophys. Res.*, 110, B01309, doi:10.1029/2004JB003104, 2005. 1633, 1637, 1638, 1639, 1640, 1648, 1649, 1651
- Pralong, A., Funk, M., and Lüthi, M. P.: A description of crevasse formation using continuum damage mechanics, *Ann. Glaciol.*, 37, 77–82, 2003. 1633, 1637, 1640
- 10 Ravi-Chandar, K. and Knauss, W.: An experimental investigation into dynamic fracture: I. Crack initiation and arrest, *Int. J. Fracture*, 25, 247–262, 1984. 1644
- Rignot, E. and Kanagaratnam, P.: Changes in the velocity structure of the Greenland Ice Sheet, *Science*, 311, 986–990, 2006. 1632
- 15 Rignot, E., Koppes, M., and Velicogna, I.: Rapid submarine melting of the calving faces of West Greenland glaciers, *Nat. Geosci.*, 3, 187–191, 2010. 1632, 1647
- Rist, M. A., Sammonds, P. R., Murrell, S. A. F., Meredith, P. G., Oerter, H., and Doake, C. S. M.: Experimental fracture and mechanical properties of Antarctic ice preliminary results, *Ann. Glaciol.*, 23, 284–292, 1996. 1643
- 20 Rist, M. A., Sammonds, P. R., Murrell, S. A. F., Meredith, P. G., Doake, C. S. M., Oerter, H., and Matsuki, K.: Experimental and theoretical fracture mechanics applied to Antarctic ice fracture and surface crevassing, *J. Geophys. Res.*, 104, 2973–2987, 1999. 1638, 1641
- Scambos, T. A., Bohlander, J., Shuman, C., and Skvarca, P.: Glacier acceleration and thinning after ice shelf collapse in the Larsen B embayment, Antarctica, *Geophys. Res. Lett.*, 31, L18402, doi:10.1029/2004GL020670, 2004. 1632
- 25 Schulson, E. M. and Duval, P.: *Creep and Fracture of Ice*, Cambridge University Press Cambridge, Cambridge, 2009. 1643
- Shepherd, A., Ivins, E. R., Geruo, A., Barletta, V. R., Bentley, M. J., Bettadpur, S., Briggs, K. H., Bromwich, D. H., Forsberg, R., Galin, N., Horwath, M., Jacobs, S., Joughin, I., King, M. A., Lenaerts, J. T. M., Li, J., Ligtenberg, S. R. M., Luckman, A., Luthcke, S. B., McMillan, M., Meister, R., Milne, G., Mouginot, J., Muir, A., Nicolas, J. P., Paden, J., Payne, A. J., Pritchard, H., Rignot, E., Rott, H., Sandberg Sørensen, L., Scambos, T. A., Scheuchl, B., Schrama, E. J. O., Smith, B., Sundal, A. V., van Angelen, J. H., van de Berg, W. J., van den

1660

- Broeke, M. R., Vaughan, D. G., Velicogna, I., Wahr, J., Whitehouse, P. L., Wingham, D. J., Yi, D., Young, D., and Zwally, H. J.: A reconciled estimate of ice-sheet mass balance, *Science*, 338, 1183–1189, 2012. 1632
- Smith, R. A.: The application of fracture mechanics to the problem of crevasse penetration, *J. Glaciol.*, 17, 223–228, 1976. 1641
- van der Veen, C.: Fracture mechanics approach to penetration of bottom crevasses on glaciers, *Cold Reg. Sci. Technol.*, 27, 213–223, 1998a. 1633, 1641, 1642, 1644
- van der Veen, C.: Fracture mechanics approach to penetration of surface crevasses on glaciers, *Cold Reg. Sci. Technol.*, 27, 31–47, 1998b. 1633, 1641, 1644
- Vaughan, D. G.: Relating the occurrence of crevasses to surface strain rates, *J. Glaciol.*, 39, 255–266, 1993. 1639
- Weiss, J.: Subcritical crack propagation as a mechanism of crevasse formation and iceberg calving, *J. Glaciol.*, 50, 109–115, 2004. 1641
- Weiss, J. and Schulson, E. M.: Coulombic faulting from the grain scale to the geophysical scale: lessons from ice, *J. Phys. D*, 42, 214017, 2009. 1639
- Xiao, J. and Jordaan, I.: Application of damage mechanics to ice failure in compression, *Cold Reg. Sci. Technol.*, 24, 305–322, 1996. 1637

1661

Table 1. Physical and numerical parameters. Tunable parameters are indicated in bold.

Parameter	Symbol	Value	Unit
Fluidity parameter	<i>A</i>		$\text{MPa}^{-3} \text{a}^{-1}$
Damage enhancement factor	<i>B</i>	0.5 to 3	Pa^{-1}
Bed friction parameter	<i>C</i>		$\text{Pa m}^{-1/3} \text{s}^{1/3}$
Crevasse depth	<i>d</i>		m
Water depth inside the crevasse	<i>d_w</i>		m
Damage variable	<i>D</i>	0 to 1	
Critical damage variable	<i>D_c</i>	0.4 to 0.6	
Glen's enhancement factor	<i>E</i>	1	
Standard gravity	<i>g</i>	9.81	ms^{-2}
Ice Thickness	<i>H</i>		m
Lateral friction coefficient	<i>k</i>		$\text{Pa m}^{-4/3} \text{a}^{1/3}$
Stress intensity factor (Mode I)	<i>K_I</i>		$\text{MPa m}^{1/2}$
Fracture toughness (Mode I)	<i>K_{Ic}</i>	0.2	$\text{MPa m}^{1/2}$
Arrest criterion (Mode I)	<i>K_{Ia}</i>		$\text{MPa m}^{1/2}$
Sea level	<i>l_w</i>		m
Bed friction exponent	<i>m</i>	1/3	
Glen exponent	<i>n</i>	3	
Deviatoric Cauchy stress tensor	<i>S</i>		Pa
Effective deviatoric Cauchy stress tensor	<i>S̄</i>		Pa
Velocity field	<i>u</i>		ms^{-1}
Channel width	<i>W</i>		m
Fracture arrest parameter	<i>α</i>	0.5	
Weigh function	<i>β</i>		$\text{m}^{-1/2}$
Strain rate	<i>ε̇</i>		
Viscosity	<i>η</i>		$\text{MPa}^{-1} \text{a}$
Water density	<i>ρ_w</i>	1000	kg m^{-3}
Ice density	<i>ρ_i</i>	900	kg m^{-3}
Cauchy stress tensor	<i>σ</i>		Pa
Effective Cauchy stress tensor	<i>σ̄</i>		Pa
Maximum principal stress	<i>σ₁</i>		Pa
Stress threshold	<i>σ_{th}</i>	20×10^3 to 200×10^3	Pa

1662

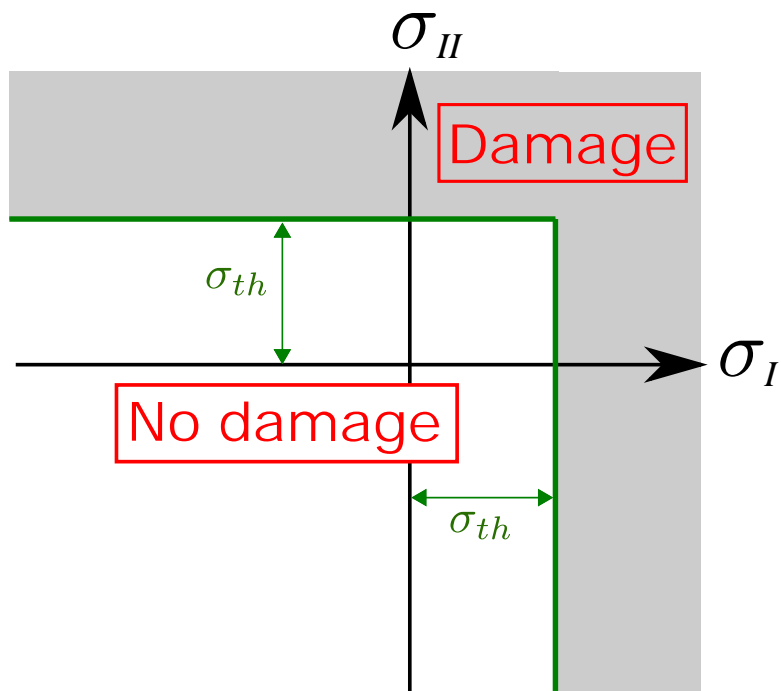


Fig. 1. Damage envelope in the space of principal stresses. σ_I and σ_{II} respectively represent the first principal stress and the second principal stress, and σ_{th} is the stress threshold. The shaded area corresponds to the stress conditions under which damage occurs.

1663

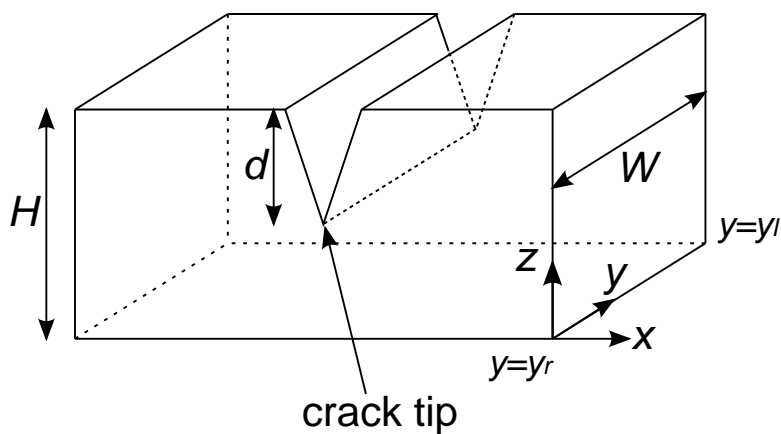


Fig. 2. Crevasse shape. H refers to the ice thickness and d is the crevasse depth.

1664

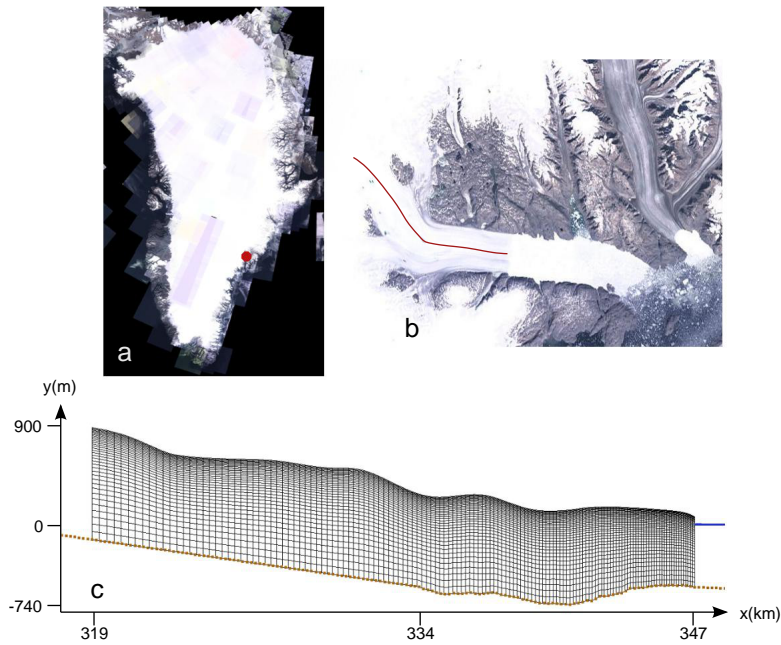


Fig. 5. Glacier location and geometry. **(a)** Location on the Greenland Ice Sheet (red point). **(b)** Zoom on the Helheim terminus and the considered flowline (red curve). **(c)** Mesh extracted from this flowline. The starting position correspond to the front position at 347 km. The blue line represents the sea level.

1667

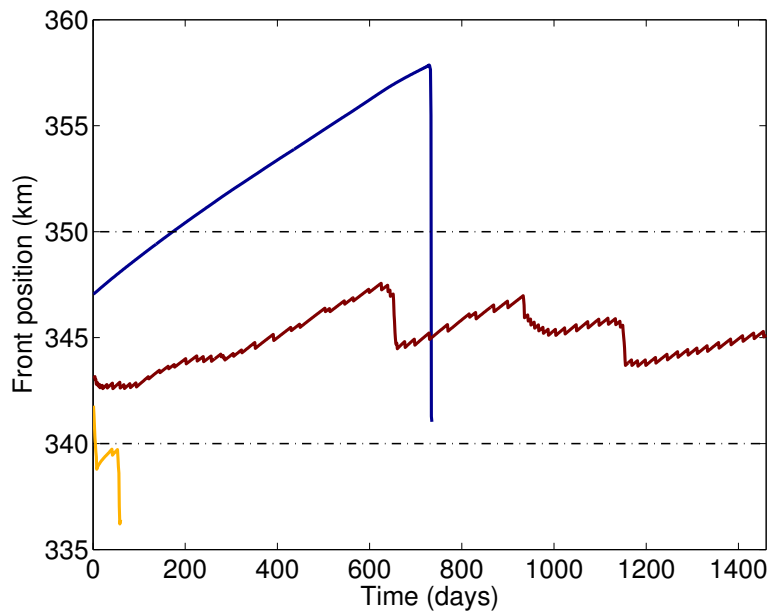


Fig. 6. Position of the calving front as a function of time. Each color correspond to a set of parameter $\bar{\sigma}_{th}$, B , and D_c . The blue color represents an advance with almost no calving ($\bar{\sigma}_{th} = 0.180$ MPa, $B = 0.878$ MPa $^{-1}$, and $D_c = 0.460$); the yellow one corresponds to a severe retreat ($\bar{\sigma}_{th} = 0.088$ MPa, $B = 2.883$ MPa $^{-1}$, and $D_c = 0.427$); the red one presents a behaviour consistent against observations ($\bar{\sigma}_{th} = 0.072$ MPa, $B = 1.870$ MPa $^{-1}$, and $D_c = 0.529$). The yellow curve stopped after 60 days because the glacier retreated too far inland. The blue curve stopped after 735 days because the glacier retreat was too large to be supported by the model.

1668

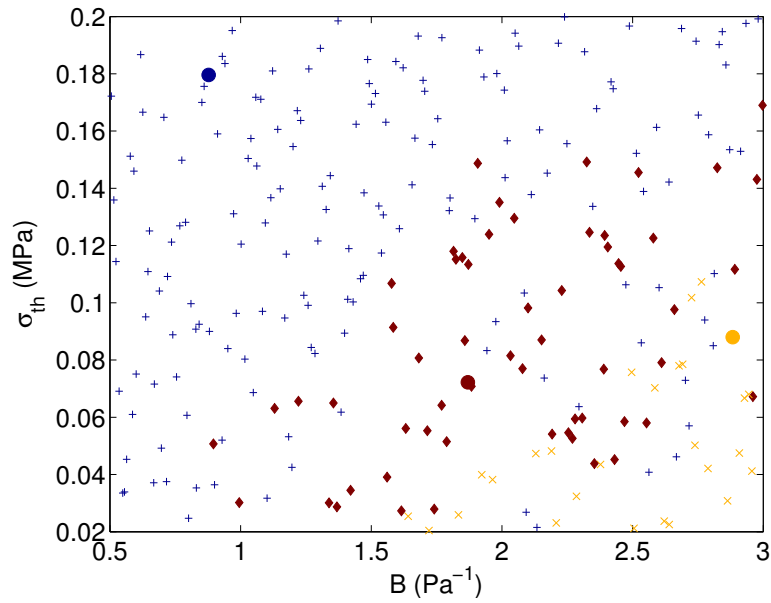


Fig. 7. Sampling in the space of damage parameters B , $\overline{\sigma}_{th}$. Blue plus signs, and yellow crosses respectively represent simulations for which the front exceed 350 km and simulation for which the front retreated below 340 km. Red diamonds represent the successful simulations. Blue, red and yellow circles corresponds to the same colored curves in Fig. 6. Red circle corresponds to the simulation illustrated on Fig. 8

1669

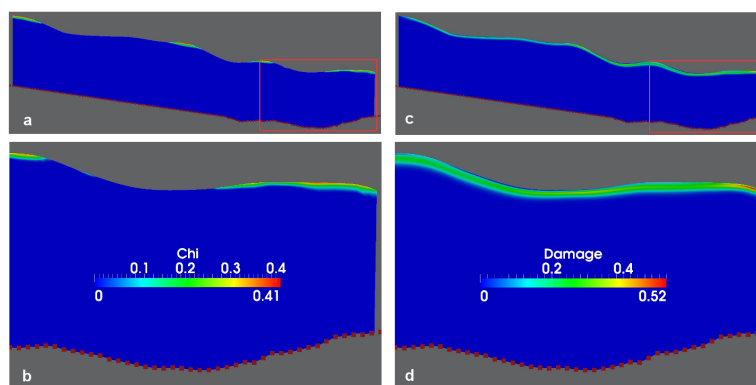


Fig. 8. State of Helheim glacier after 365 days of simulation for the set of parameter ($\overline{\sigma}_{th} = 0.072$ MPa, $B = 1.870$ MPa $^{-1}$, and $D_c = 0.529$) corresponding to the red circle on Fig. 7. **(a)** Damaging areas of Helheim glacier and **(b)** zoom on the red rectangle; **(c)** damage field and zoom on the red rectangle **(d)**.

1670

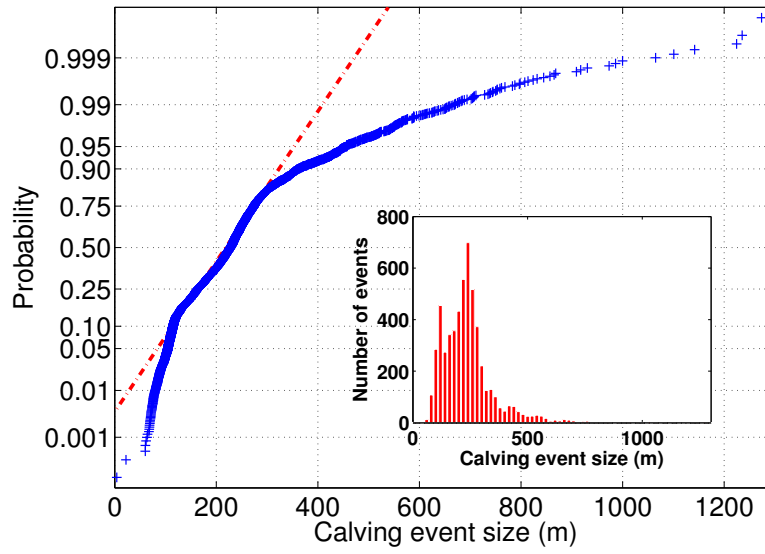


Fig. 9. Gaussian anamorphosis for the sizes of calving events corresponding to the 59 realistic simulations. Dashed-red curves represents the gaussian distribution associated with the calving event size distribution. Blue crosses correspond to individual events. The corresponding classical histogram is shown in the inset.